ACS OMEGA

http://pubs.acs.org/journal/acsodf

Article

Spirooxazine-Based Dual-Sensing Probe for Colorimetric Detection of Cu^{2+} and Fe^{3+} and Its Application in Drinking Water and Rice Quality Monitoring

Supak Pattaweepaiboon, Weerapat Foytong, Natchayapak Phiromphu, Tanin Nanok, Narongpol Kaewchangwat, Khomson Suttisintong,* and Weekit Sirisaksoontorn*

Cite This: *ACS Omega* 2022, 7, 18671−18680

Read Online

ACCESS | Metrics & More | Article Recommendations | Supporting Information

ABSTRACT: A spirooxazine derivative, **PheSPO** (3,3-dimethyl-1-phenethylspiro-[indoline-2,3′-naphtho[2,1-*b*][1,4]oxazine]), as a dual-sensing probe for Cu^{2+} and Fe^{3+} was synthesized, and its structure was confirmed by ^{1}H NMR, ^{13}C NMR, HRMS, and single-crystal X-ray diffraction. The results reveal that the **PheSPO** probe is selective to both Cu^{2+} and Fe^{3+} through distinct colorimetric responses in acetonitrile. The sensing performance of **PheSPO** toward Cu^{2+} was investigated, and upon addition of Cu^{2+}, an instant change in color from colorless to bright yellow with a strong absorption band at 467 nm was observed. Due to a dual-sensing behavior, **PheSPO** also exhibits a unique response toward Fe^{3+} that can be discovered from a color change from colorless to red at an absorption wavelength of 514 nm. Based on spectroscopic analyses and density functional theory calculations, the 1:1 stoichiometric complexation of **PheSPO** with the targeted metal ions was proposed and the binding constants of 1.95×10^3 M^{-1} for Cu^{2+} and 1.29×10^3 M^{-1} for Fe^{3+} were obtained. In addition, the detection limits of **PheSPO** for Cu^{2+} and Fe^{3+} were 0.94 and 2.01 μM, respectively. To verify its applicability in real samples, **PheSPO** was further explored for quantitative determination of both Cu^{2+} and Fe^{3+} in spiked drinking water. The results showed that the recoveries of Cu^{2+} and Fe^{3+} examined using the **PheSPO** probe were found comparable to those obtained from atomic absorption spectroscopy. Moreover, the **PheSPO** strip test was developed, and its utilization for qualitative detection of Fe^{3+} in real rice samples was demonstrated.

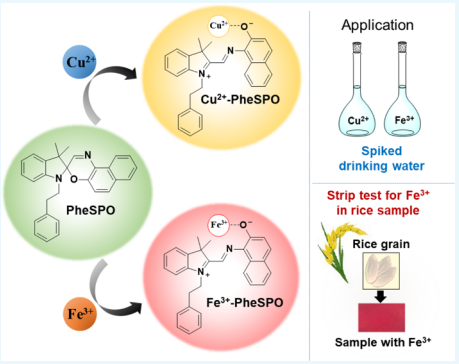

1. INTRODUCTION

Among essential transition metal ions, Cu^{2+} and Fe^{3+} are vital for biological processes including catalysis, metabolism, and signaling.[1−3] Under physiological imbalance, these metal ions can lead to diverse health problems.[4−7] Although Cu^{2+} plays a crucial role in ATP production, catecholamine biosynthesis, and protecting the cells from oxygen-free radicals,[8−10] disturbance in homeostasis of Cu^{2+} can be highly poisonous to cells and has been linked to the predominance of neurodegenerative diseases such as Menkes,[11] Wilson's,[12] Alzheimer's,[13] and Parkinson's diseases.[14] Moreover, these chronic diseases can originate from both the deficiency and excess of Fe^{3+} despite its necessity for enzyme catalysis in cellular metabolism.[15,16] As a consequence, the US EPA has recommended that the dietary intake of Cu^{2+} and Fe^{3+} should not exceed the maximum allowable concentrations in food (Cu^{2+}, 1.0−1.3 mg/day for adults and Fe^{3+}, 19.3−20.5 mg/day in men and 17.0−18.9 mg/day in women) and water (Cu^{2+}, 1.3 mg/L and Fe^{3+}, 0.3 mg/L).[17−19] Ordinarily, the capability of measuring the quantity of Cu^{2+} and Fe^{3+} in biological and environmental samples is exemplified by the conventional methods, including atomic absorption spectroscopy (AAS),[20,21] inductively coupled plasma mass spectrometry (MS),[22,23] and ion chromatography.[24,25] These methods, however, are rather complicated, time-consuming, and costly, especially for inexperienced users. Therefore, many researchers have focused on the development of an applicable and reliable approach for the detection of Cu^{2+} and Fe^{3+} by using a chemosensor.[26−28]

A chemosensor is a molecular probe that empowers the transformation of analyte information into a measurable signal of colorimetric or fluorescent responses.[29] Much effort has been drawn to develop chemosensors with efficient sensing performance for rapid and accurate detection.[30] To obtain an improved selectivity and sensitivity for the analysis of metal ions, a particular part of the chemosensors is designed for specific binding with the metal-ion analyte. This subsequently leads to a spectral change in their signals and sometimes a

Received: March 6, 2022
Accepted: May 17, 2022
Published: May 25, 2022

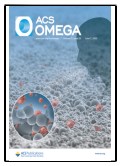

structural change can be observed in some chemosensors.[31] Several organic molecules, for example, rhodamine, anthracene, benzothiadiazole, squaraine, and phenothiazine, have been studied as potential chemosensors to detect a wide range of metal ions.[32−36] Moreover, their sensing mechanism in response to metal ions was also proposed based on the metal−ligand coordination and chemical reactions, such as bond cleavage, bond formation, rearrangement, and cyclization.[37] To date, several chemosensors as colorimetric probes with high selectivity and sensitivity as a facile and rapid tool for on-site analysis of metal ions have been reported.[38−42]

Owing to its unique optical property, spirooxazine has shown the capability as a chemosensor in response to metal ions.[43] The specific ion recognition modulated by spirooxazine occurs via ring opening together with metal−ligand complexation. Typically, the ring-opening reaction of spirooxazine proceeds through bond cleavage at the spiro carbon (C_{spiro}−O), which is induced by either electromagnetic radiation or metal ion stimuli.[44,45] This process results in the formation of an open-ring form, also known as merocyanine, which can serve as an active ligand to selectively coordinate with a metal ion and produce a merocyanine−metal complex.[46] Recently, some spirooxazine probes showed high selectivity for the detection of metal ions, including Mg^{2+}, Al^{3+}, Fe^{3+}, Co^{2+}, Zn^{2+}, Hg^{2+}, and CH_3Hg^+.[47−53] However, few studies of spirooxazine probes for Cu^{2+} detection have been described, and to the best of our knowledge, the spirooxazine as a dual probe for Cu^{2+} and Fe^{3+} detection has not yet been reported.

Herein, we demonstrated the utilization of a spirooxazine derivative, 3,3-dimethyl-1-phenethylspiro[indoline-2,3′-naphtho[2,1-*b*][1,4]oxazine] (**PheSPO**), as a dual-sensing probe that possessed high selectivity and sensitivity toward Cu^{2+} and Fe^{3+} in acetonitrile. Its synthesis is presented in Schemes 1 and 2 in three steps of the longest linear sequence.

Scheme 1. Preparation of Zinc Complex 2

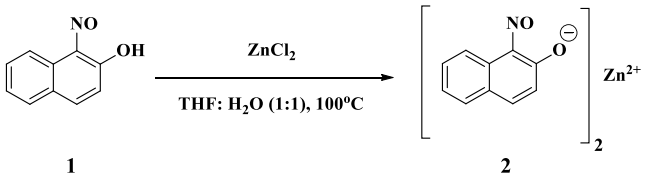

The sensing performance of **PheSPO** against Cu^{2+} and Fe^{3+} was determined by a distinct change in color at the micromolar level. To prove that **PheSPO** can be applied in practical application, the probe was further used to detect the trace amount of Cu^{2+} and Fe^{3+} in spiked drinking water. Moreover, the test strips of **PheSPO** were also fabricated for qualitative detection of Fe^{3+} in rice samples.

2. EXPERIMENTAL SECTION

2.1. Materials and General Information. 1-Nitroso-2-naphthol, zinc chloride, (2-bromoethyl)benzene, 2,3,3-trimethylindolenine, and triethylamine were purchased from Tokyo Chemical Industry (TCI). Tetrahydrofuran, acetonitrile, dichloromethane, and ethanol were obtained from Honeywell Burdick & Jackson (B&J). Metal ions including Na^+, K^+, Mg^{2+}, Ca^{2+}, Sr^{2+}, Ba^{2+}, Sn^{2+}, Pb^{2+}, Cr^{3+}, Mn^{2+}, Fe^{2+}, Fe^{3+}, Co^{2+}, Ni^{2+}, Cu^{2+}, Zn^{2+}, Cd^{2+}, and Hg^{2+} were obtained from Sigma-Aldrich as chloride salts. All reagents were of analytical grade and used as received unless stated otherwise. Deionized water (DI) was used for all experiments. Analytical thin-layer chromatography (TLC) was performed on Kieselgel F_{254} pre-coated aluminum TLC plates obtained from EM Science. Visualization was performed with a 254 nm ultraviolet lamp. Column chromatography was carried out with Merck silica gel 60 (230−400 mesh ASTM). UV/vis absorption spectra were measured on a Shimadzu (UV-1800) spectrophotometer at ambient temperature. The path length of a quartz cell was 1 cm. ^{1}H NMR (500 MHz) and ^{13}C NMR (125 MHz) spectra with entire proton decoupling were recorded on a Bruker AVANCE 500 NMR spectrometer, and chemical shifts in ppm were quoted relative to the residual signals of deuterated solvents. High-resolution mass spectra were recorded using a Bruker micrOTOF mass spectrometer (ESI-TOF) and reported with ion mass/charge (m/z) ratios as values in atomic mass units.

2.2. Synthesis of PheSPO. *2.2.1. 1-Nitroso-2-naphthol Zinc Salt (2).* To a stirred solution of 1-nitroso-2-naphthol (**1**) (5.00 g, 28.87 mmol) in a mixture of tetrahydrofuran and water (1:1 v/v) (130 mL) was added zinc chloride (1.64 g, 12.03 mmol) in one portion, and the resulting mixture was heated to 100 °C and stirred at this temperature for 2 h. The reaction mixture was cooled to room temperature, and the suspension was filtered. The precipitate was washed with cold water and dried under a vacuum for 24 h to give 1-nitroso-2-naphthol zinc salt (**2**) as a brown solid (4.58 g). This crude product was used in the next step without purification.

2.2.2. 3,3-Dimethyl-2-methylene-1-phenethylindoline (6). To a stirred solution of (2-bromoethyl)benzene (4.60 g, 24.87 mmol) in acetonitrile (120 mL) under an Ar atmosphere was added 2,3,3-trimethylindolenine (3.96 g, 24.87 mmol). The reaction mixture was heated to reflux with stirring for 48 h. The mixture was cooled to room temperature, and the solvent was evaporated under reduced pressure. The resulting viscous oil was washed with diethyl ether (2 × 60 mL) and dried under a vacuum for 12 h to give indolium salt **5**, which was dissolved in dichloromethane (120 mL). To the resulting solution was added triethylamine (7.55 g, 74.60 mmol), and the mixture was stirred at room temperature for 8 h. The reaction mixture was washed with water (2 × 75 mL) and the organic layer was dried over anhydrous Na_2SO_4, filtered, and concentrated under reduced pressure. The residue was purified by column chromatography (5% ethyl acetate in hexane) to afford the title product (**6**) as a red oil (5.24 g, 80%). ^{1}H NMR (500 MHz, $CDCl_3$): δ 7.31−7.20 (m, 5H), 7.10−7.07 (m, 2H), 6.74 (t, J = 7.4 Hz, 1H), 6.46 (d, J = 8.0 Hz, 1H), 3.92 (s, 1H), 3.86 (d, J = 2.0 Hz, 1H) 3.70 (t, J = 7.8 Hz, 2H), 2.89 (t, J = 7.8 Hz, 2H), 1.33 (s, 6H); HRMS (ESI) m/z: calcd for $C_{19}H_{22}N$ [M + H]$^+$, 264.3847; found, 264.1752.

2.2.3. 3,3-Dimethyl-1-phenethylspiro[indoline-2,3′-naphtho[2,1-b][1,4]oxazine] (7, PheSPO). To a stirred solution of 1-nitroso-2-naphthol zinc salt **2** (2.14 g, about 9 mmol) in ethanol (70 mL) under an Ar atmosphere was added indoline **6** (2.00 g, 7.6 mmol), and the resulting mixture was heated to reflux for 8 h. The mixture was cooled to room temperature, and the solvent was removed under reduced pressure. The residue was purified by column chromatography (40% dichloromethane in hexane) to afford **PheSPO** (1.18 g, 37%) as a green solid. ^{1}H NMR (500 MHz, CD_3OD): δ 8.44 (d, J = 10.5 Hz, 1H), 7.76 (d, J = 10.2 Hz, 1H), 7.70 (d, J = 11.1 Hz, 1H), 7.54 (dd, J = 8.6, 1.4 Hz, 1H), 7.38 (dd, J = 10.1, 1.4 Hz, 1H), 7.25−7.17 (m, 4H), 7.07 (dd, J = 9.1, 0.9 Hz, 1H), 7.04−7.02 (m, 2H), 6.99 (s, 1H), 6.97 (d, J = 11.1

https://doi.org/10.1021/acsomega.2c01353
ACS Omega 2022, 7, 18671−18680

Scheme 2. Synthesis of PheSPO

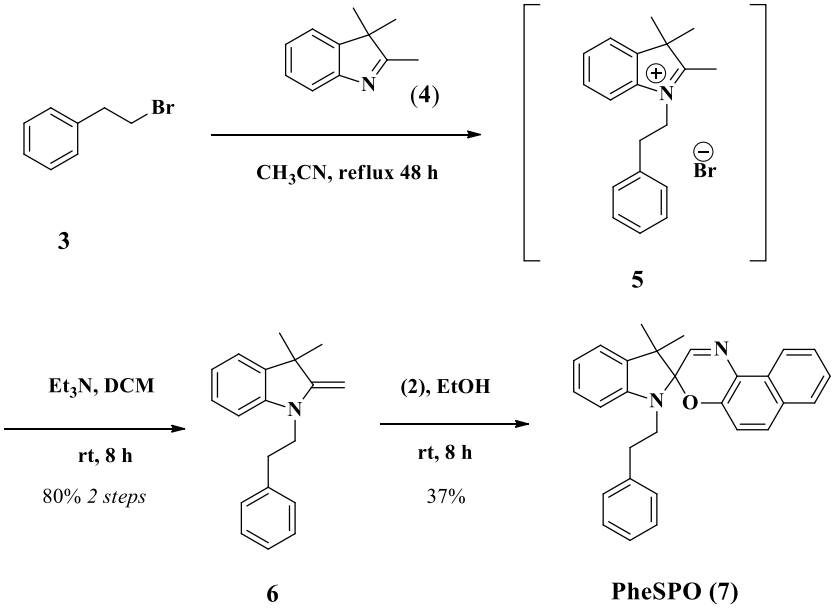

Hz, 1H), 6.86 (t, J = 9.2 Hz, 1H), 6.71 (d, J = 9.7 Hz, 1H), 3.44−3.35 (m, 2H), 3.07−2.99 (m, 1H), 2.82−2.76 (m, 1H), 1.25 (s, 3H), 1.19 (s, 3H); ^{13}C NMR (125 MHz, CD_3OD): δ 151.3, 146.5, 143.9, 139.6, 135.6, 130.5, 130.0, 129.4, 128.9, 128.0, 127.6, 127.5, 126.7, 126.0, 123.8, 122.6, 121.1, 121.0, 119.3, 116.4, 106.5, 98.8, 51.8, 46.3, 34.5, 24.4, 19.6; HRMS (ESI) m/z: calcd for $C_{29}H_{26}N_2ONa$ $[M + Na]^+$, 441.1943; found, 441.1937.

2.3. Single-Crystal Analysis. 20.9 mg of **PheSPO** was gently dissolved in 5 mL of 1,4-dioxane with the assistance of sonication for 5 min at 40 °C. Then, 3 mL of DI water was slowly dropped into the solution. After slow evaporation of the solvent under ambient temperature for 2 weeks, a colorless single crystal of **PheSPO** was obtained for analysis. The X-ray diffraction intensity data were collected on a Bruker D8 Venture geometry diffractometer with Cu Kα radiation (λ = 1.54178 Å) at room temperature. A complete structure solution of the **PheSPO** single crystal was performed on Olex2 software.

2.4. UV−Visible Absorption Study. The stock solutions of **PheSPO** (0.1 mM) and metal ions (0.1 mM), including Na^+, K^+, Mg^{2+}, Ca^{2+}, Sr^{2+}, Ba^{2+}, Sn^{2+}, Pb^{2+}, Cr^{3+}, Mn^{2+}, Fe^{2+}, Fe^{3+}, Co^{2+}, Ni^{2+}, Cu^{2+}, Zn^{2+}, Cd^{2+}, and Hg^{2+}, were freshly prepared in acetonitrile and stored in dark for further use. The spectral change of the mixed solutions of **PheSPO** (50 μM) and metal ions (50 μM) was monitored on a Shimadzu UV-1800 spectrophotometer operated at room temperature. The quartz cuvettes with 1 cm path length were used.

2.5. DFT Calculations. The ground-state geometries of **PheSPO** in its open form and its complexation with cationic species in an implicit solvent model of acetonitrile were fully optimized at the density functional theory (DFT) level of theory using the B3LYP hybrid functional[54,55] with the DFT-D3 dispersion correction.[56,57] The 6-311+G(d,p) and def2-tzvp basis sets were used to describe the electronic configurations of nonmetal and metal atoms, respectively. The solvent effects of acetonitrile (with a dielectric constant ε = 35.688) were accounted for using the polarizable continuum model.[58,59] The optimized geometries and frontier molecular orbitals were visualized with ChemCraft software.[60] All calculations were performed using the Gaussian 09 suite of programs.[61]

2.6. Analysis of Cu^{2+} and Fe^{3+} in Drinking Water. To determine the optimal conditions for **PheSPO** in detecting Cu^{2+} and Fe^{3+} in drinking water, the effect of solvent polarity was studied in detail, and the results are discussed in the Supporting Information (Figure S1).

In brief, 5 mL of drinking water obtained from a water dispenser was spiked with known concentrations of Cu^{2+} and Fe^{3+}. The spiked solution was made up to 10 mL with DI water in a volumetric flask. Then, 2 mL of the spiked solution was thoroughly mixed with 2 mL of 20 μM **PheSPO** in acetonitrile. The mixed solution was irradiated with 395 nm UV light for 5 min. The colorimetric response of the solution was monitored by UV−visible spectroscopy.

To evaluate the efficiency and accuracy of the **PheSPO** probe, the concentrations of Cu^{2+} and Fe^{3+} in the spiked sample were also analyzed by standard flame AAS operated on a PerkinElmer AAnalyst 200 system.

2.7. Strip Test for Fe^{3+} Detection in Rice. The test strips of the **PheSPO** probe for Fe^{3+} detection were prepared by immersing TLC plates (1 × 1 cm^2) into a solution of **PheSPO** (1 mM) in acetonitrile for 5 min, and the resulting wet strips were dried in air. To optimize the analysis conditions for the strip test, the sensing performance of **PheSPO** coated on a TLC plate in detecting Cu^{2+} and Fe^{3+} was investigated under various pH conditions, and the results are shown in Figure S2.

The rice sample was prepared as follows: 5 g of ground rice (Khao Dawk Mali 105) was added to a 50 mL block digestion tube, which contained 6 mL of a mixture of 37% HCl and 70% $HClO_4$ (2:1, v/v). The resulting mixture was heated at 180 °C for 6 h. After digestion was completed, the clear solution was transferred into a volumetric flask and made up to 10 mL with ultrapure water. The stock solution of the digested rice sample was kept in dark for further Fe^{3+} analysis.

To evaluate the presence of Fe^{3+} in the rice, a drop of the digested rice sample was cast on the **PheSPO**-treated strips, and the change in color was observed by the naked eye.

https://doi.org/10.1021/acsomega.2c01353
ACS Omega 2022, 7, 18671−18680

3. RESULTS AND DISCUSSION

3.1. Single Crystal of PheSPO. The single crystal of **PheSPO** was grown through slow evaporation of solvents, and it crystallized in the monoclinic space group $P2_1/c$. The crystallographic data are reported in Table S1 and deposited at CCDC (no. 2154731). As shown in Figure 1, the molecular

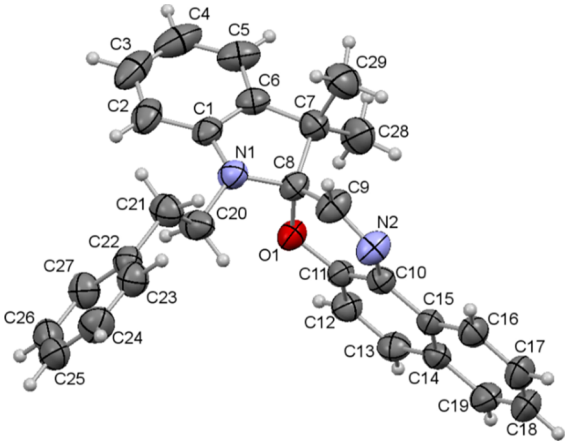

Figure 1. ORTEP diagram of **PheSPO** at 50% probability displacement of the ellipsoids.

structure of **PheSPO** contains two heterocyclic rings of indoline and oxazine fragments that are mutually orthogonal to each other and connected through the sp^3-hybridized spiro carbon (C8). The O1−C8 bond length is 1.4578 Å, which is slightly longer than that of typical oxygen-containing heterocycles (1.41−1.43 Å). Upon exposure to the external stimuli, the cleavage of the O1−C8 bond in **PheSPO** via ring-opening reaction is activated. This subsequently leads to the formation of an open-form merocyanine.

3.2. UV−Visible Absorption Study. The selectivity of **PheSPO** was investigated against various metal ions, including Na^+, K^+, Mg^{2+}, Ca^{2+}, Sr^{2+}, Ba^{2+}, Sn^{2+}, Pb^{2+}, Cr^{3+}, Mn^{2+}, Fe^{2+}, Fe^{3+}, Co^{2+}, Ni^{2+}, Cu^{2+}, Zn^{2+}, Cd^{2+}, and Hg^{2+} in acetonitrile solutions. In Figure 2, the results clearly show the change in color of **PheSPO** solutions from colorless to red for Fe^{3+} treatment and from colorless to yellow for Cu^{2+} treatment. On the contrary, the mixed solutions remained colorless upon the treatment with other metal ions. This indicates that **PheSPO** can provide a selective response against Cu^{2+} and Fe^{3+} with a distinct change in color that can be seen with the naked eye. In addition, the spectral change of **PheSPO** upon addition of metal ions was further evaluated by UV−visible absorption. As shown in Figure 3, free **PheSPO** exhibits two main absorption peaks at 317 and 349 nm due to the $\pi \rightarrow \pi^*$ transition of the naphthooxazine ring.[62] Addition of Cu^{2+} into the **PheSPO** solution caused an emergence of a relatively strong absorption

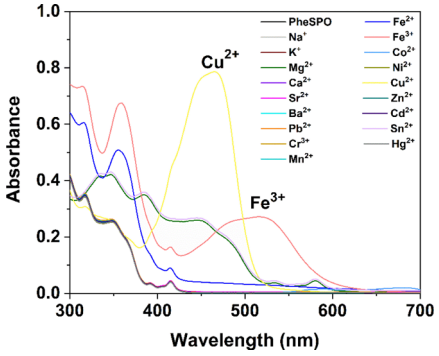

Figure 3. UV−visible absorption spectra of **PheSPO** (50 μM) in acetonitrile in the presence of various metal ions (50 μM).

band at λ_{max} 467 nm. Meanwhile, the **PheSPO** solution mixed with Fe^{3+} displays a new absorption band at λ_{max} 514 nm. These two bands of absorption in the visible region are mainly ascribed to the formation of the open-form merocyanine with extended π-conjugation induced by the complexation with Cu^{2+} and Fe^{3+}. In the case of other metal ions, no significant change in the absorption spectra was observed. These results suggest that **PheSPO** can act as a dual-sensing probe for the detection of Cu^{2+} and Fe^{3+}.

To examine the selectivity of the **PheSPO** probe toward Cu^{2+} and Fe^{3+} detection, competitive experiments in acetonitrile solutions were carried out in the presence of other interfering metal ions. As shown in Figure 4a where the selectivity of **PheSPO** toward Cu^{2+} is investigated, the absorbance change at 467 nm of other cations was negligible when compared to that of **PheSPO** mixed with Cu^{2+}. This suggests that the coexistence of other metal ions has insignificant effect on the sensing performance of **PheSPO** toward Cu^{2+}. In the case of **PheSPO** and Fe^{3+}, Cu^{2+} was the only metal ion that exhibited significant interference to the absorbance at 514 nm (Figure 4b). A marked decrease in absorbance at 514 nm when Cu^{2+} was added to the solution of **PheSPO** and Fe^{3+} might be the result from the replacement of Fe^{3+} in the Fe^{3+}−**PheSPO** complex with Cu^{2+}. To confirm our proposal, the spectral change of **PheSPO** and Fe^{3+} solution was monitored with increasing addition of Cu^{2+}, and the results in Figure 5 show an increase in absorbance at 467 nm (Cu^{2+}−**PheSPO**) along with a simultaneous decrease in absorbance at 514 nm (Fe^{3+}−**PheSPO**). This suggests that Cu^{2+} could generate considerable interference against Fe^{3+} detection with the **PheSPO** probe in mixed metal-ion solutions.

The complexation stoichiometry of **PheSPO** and metal ions (Cu^{2+} and Fe^{3+}) was studied by using Job's method. The equimolar solutions of **PheSPO** and metal ions were prepared with different mole fractions, and Job's plots were established using the absorbance of 467 nm for Cu^{2+} and 514 nm for Fe^{3+}

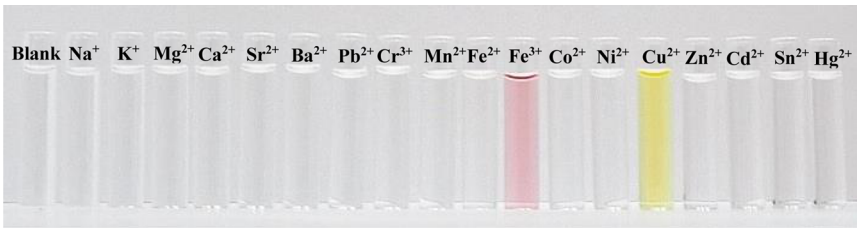

Figure 2. Photograph of colorimetric responses of PheSPO (50 μM) in acetonitrile in the presence of various metal ions (50 μM).

https://doi.org/10.1021/acsomega.2c01353
ACS Omega 2022, 7, 18671−18680

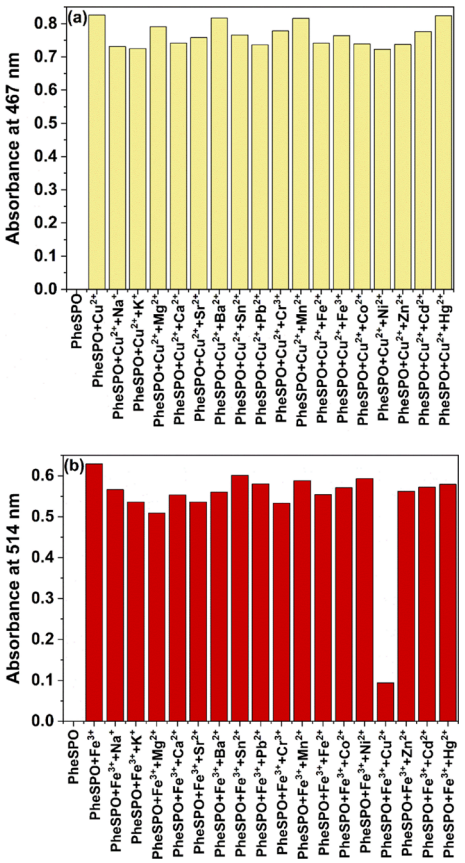

Figure 4. Selectivity of **PheSPO** (50 μM) in acetonitrile toward (a) Cu^{2+} and (b) Fe^{3+} (5 equiv) in the presence of other interfering metal ions (5 equiv).

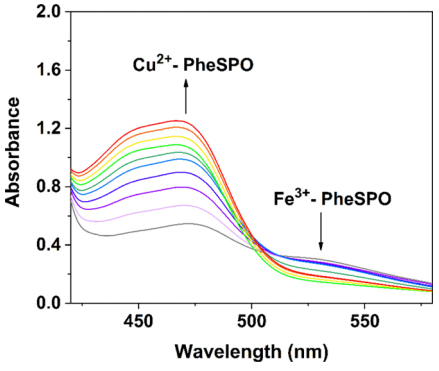

Figure 5. Spectral change of the solution of **PheSPO** (2 mM) and Fe^{3+} (50 μM) in acetonitrile upon increasing addition of Cu^{2+} (50–300 μM).

as shown in Figure 6a,b, respectively. The maximum absorbance at a mole fraction of 0.5 in both cases suggests that the metal–**PheSPO** complex occurs at a 1:1 stoichiometric ratio. Therefore, the reaction mechanism for the ring opening of **PheSPO** in the presence of Cu^{2+} or Fe^{3+} (represented as M^{n+}) was proposed based on the 1:1 complex formation as shown in Figure 7. This metal ion-induced ring opening of **PheSPO** takes place via bond cleavage at the spiro carbon and liberates the phenolate oxygen (Ph–O^-), which subsequently coordinates to metal ions through the vacancy site. This process also causes a unique change in the optical behavior of **PheSPO** due to the effect of extended π-

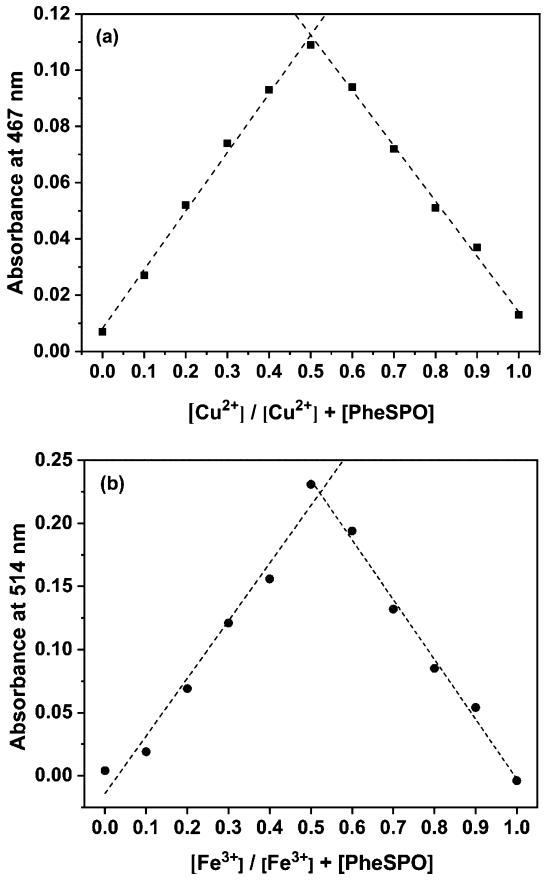

Figure 6. Job's plots for the determination of complexation stoichiometry of acetonitrile solutions of (a) **PheSPO** and Cu^{2+} and (b) **PheSPO** and Fe^{3+}. The total concentration was fixed at 10 μM.

conjugation of open-form merocyanine after bond breaking reaction and metal complexation. In addition, the MS spectra of metal–**PheSPO** complexes in Figure S3 also show the molecular peaks at 497.1338 m/z and 509.1144 m/z, which correspond to the presence of [**PheSPO**–$2H^+$ + Cu^{2+} + H_2O] and [**PheSPO**–H^+ + Fe^{3+} + $2H_2O$], respectively. These results clearly confirm the complex formation of **PheSPO** with the targeted metal ions (Cu^{2+} and Fe^{3+}).

The sensitivity of **PheSPO** for the detection of Cu^{2+} and Fe^{3+} was also examined to evaluate the detection limits. This was conducted by the absorption titration with the concentration of metal ions ranging from 0 to 1 equiv. The results in Figure 8a,b reveal that the absorbance at the wavelength corresponding to the complexation gradually increased with increasing metal-ion concentrations. Moreover, the absorbance changes of **PheSPO** versus Cu^{2+} and Fe^{3+} concentrations exhibit a good linear relationship with $R^2 > 0.99$ as shown in the insets. Based on the linear response observed, the detection limits derived from $3\sigma/m$, where σ is the standard deviation of blank measurements and m is the slope of a plot between absorbance versus metal-ion concentration, were found to be 0.94 μM for Cu^{2+} and 2.01 μM for Fe^{3+}. This demonstrates that the **PheSPO** dual-sensing probe possesses high sensitivity toward Cu^{2+} and Fe^{3+} detection when compared to the previously reported dual-sensing probes (see Table S2).

According to the 1:1 reaction stoichiometry, the binding constant (K_α) was evaluated by using the Benesi–Hildebrand

https://doi.org/10.1021/acsomega.2c01353
ACS Omega 2022, 7, 18671–18680

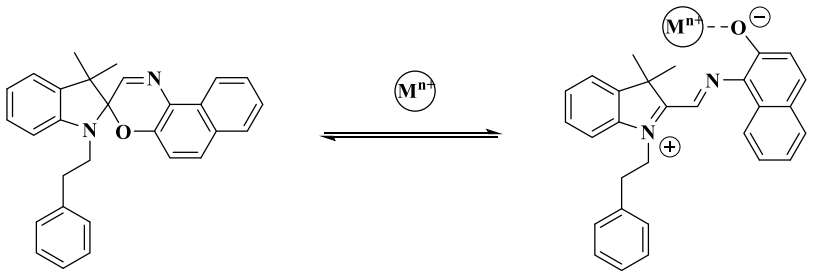

Figure 7. Proposed metal ion-induced ring-opening reaction of **PheSPO** in the presence of the targeted metal ions (M^{n+} = Cu^{2+} or Fe^{3+}).

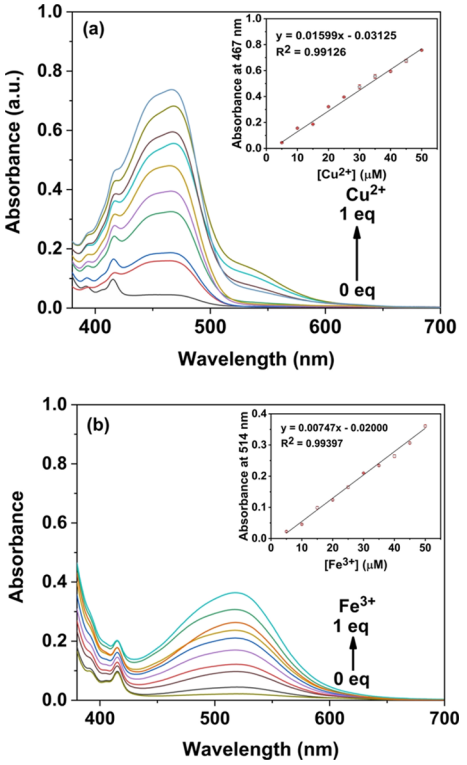

Figure 8. Spectral changes of PheSPO (50 μM) in acetonitrile with increasing addition (0−1 equiv) of (a) Cu^{2+} and (b) Fe^{3+}. The insets show a linear response with the increase in Cu^{2+} and Fe^{3+} concentrations.

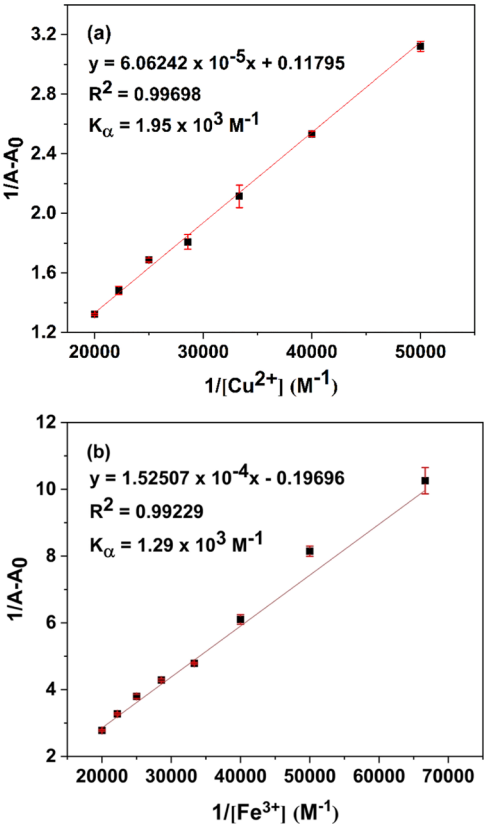

Figure 9. Benesi−Hildebrand plots of the 1:1 stoichiometric ratio of (a) **PheSPO** and Cu^{2+} and (b) **PheSPO** and Fe^{3+}.

equation: $\frac{1}{A-A_0} = \frac{1}{K_\alpha(A_{max}-A_0)[C]} + \frac{1}{A_{max}-A_0}$, where A and A_0 are the absorbance of **PheSPO** in the presence and absence of metal ions, respectively, A_{max} is the saturated absorbance of **PheSPO** in the presence of an excess amount of metal ions, and [C] is the concentration of metal ions. The resulting plots in Figure 9a,b show the best fit of the linear function with R^2 > 0.99, and the K_α values of the complexes were found to be 1.95 × 10^3 M^{-1} for Cu^{2+} and 1.29 × 10^3 M^{-1} for Fe^{3+}.

3.3. Computational Study. To gain insight into the structures and absorption behaviors of **PheSPO** and its 1:1 complex with metal ions, DFT calculations were performed at the B3LYP-D3 level with hybrid basis sets of 6-311+G(d,p) and def2-tzvp. The optimized structures of free **PheSPO** and the resulting complexes with Cu^{2+} and Fe^{3+} are shown in Figure 10a. The result suggests that in the absence of metal ions, the free **PheSPO** remains stable in a closed form in which the oxazine ring is arranged orthogonally with the indoline ring through a spiro carbon linkage. Upon complexation, the optimized geometry of **PheSPO** turned into open-form merocyanine with the planar TTC (trans−trans−cis) conformation, of which the oxygen phenolate anion plays an important role in binding with the metal-ion center. According to the DFT results, the optimized complex contains monodentate **PheSPO** together with water and chloride ligands in binding with Cu^{2+} in square planar and Fe^{3+} in octahedral coordination geometry.

In Figure 10b, the frontier molecular orbitals of free closed-form **PheSPO** exhibit the localization of π-electrons on the indoline fragment, and the calculated energy gap between the highest occupied molecular orbital (HOMO) and lowest unoccupied molecular orbital (LUMO) was found to be 3.77 eV. On the contrary, in the case of the metal−**PheSPO** complex, the open-form merocyanine can facilitate π-electron delocalization throughout the molecule, giving rise to a significant decrease in energy gap for the electronic transition from the HOMO to LUMO, that is, 2.54 eV (488 nm) for Cu^{2+}−**PheSPO** and 2.34 eV (530 nm) for Fe^{3+}−**PheSPO**. These DFT calculation results are consistent with the

https://doi.org/10.1021/acsomega.2c01353
ACS Omega 2022, 7, 18671−18680

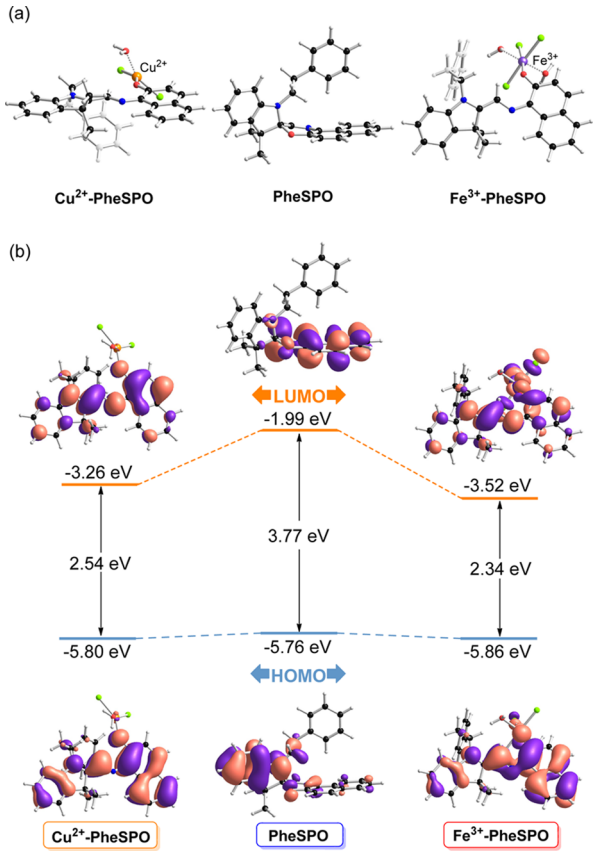

Figure 10. (a) Optimized structures and (b) frontier molecular orbitals of free **PheSPO**, Cu^{2+}−**PheSPO**, and Fe^{3+}−**PheSPO** complexes calculated at the B3LYP-D3 level using hybrid basis sets 6-311+G(d,p) for H, C, N, O, and Cl and def2-tzvp for Cu and Fe.

absorption spectra and also confirm the proposed metal ion-induced ring-opening reaction of **PheSPO** in the presence of Cu^{2+} and Fe^{3+}.

3.4. Analysis of Cu^{2+} and Fe^{3+} in Drinking Water. To verify that the **PheSPO** dual-sensing probe can be employed as a sensing tool in the practical application, it was used to determine the amounts of Cu^{2+} and Fe^{3+} in spiked drinking water. The results in Table 1 show that %recovery of Cu^{2+} analyzed with **PheSPO** was in the range of 93−97% at the micromolar concentrations. Meanwhile, %recovery of Fe^{3+} exceeded 100%, which may result from the background concentration of Fe^{3+} existing in drinking water. Impressively, the results obtained from the **PheSPO** probe were comparable to those obtained from the standard AAS. Therefore, it is obvious that **PheSPO** can be practically used as a colorimetric probe for accurate detection of Cu^{2+} and Fe^{3+} in drinking water.

Table 1. % Recoveries of Cu^{2+} and Fe^{3+} in Drinking Water

		$[Cu^{2+}]_{found}$ (μM)			
sample	$[Cu^{2+}]_{added}$ (μM)	**PheSPO**	% recovery	AAS	% recovery
1	3.00	2.81	93.63	2.88	96.08
2	7.00	6.83	97.55	6.99	99.84
		$[Fe^{3+}]_{found}$ (μM)			
sample	$[Fe^{3+}]_{added}$ (μM)	**PheSPO**	% recovery	AAS	% recovery
1	3.00	3.15	105.00	3.04	101.40
2	7.00	7.67	109.57	7.50	107.08

3.5. Strip Test for Fe^{3+} Detection in Rice. The **PheSPO** test strip coated on a TLC plate was fabricated and used for qualitative detection of Fe^{3+} in the digested solution of the rice sample. In Figure 11, the **PheSPO** test strip shows a distinct color change from pale greenish blue to red when treated with the sample solution. In the case of the acid control, the **PheSPO** test strip remains unchanged in color. This confirms the colorimetric response of **PheSPO** to the existence of Fe^{3+} in rice, in which the actual amount of Fe^{3+} in the sample solution was 87.62 μM as determined by AAS. Thus, the **PheSPO** test strip is apparently applicable for qualitative detection of Fe^{3+} in rice.

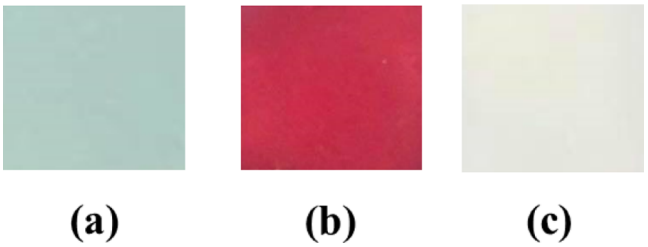

Figure 11. Photographs of (a) **PheSPO** test strip, (b) **PheSPO** test strip treated with the digested solution of the rice sample, and (c) **PheSPO** test strip treated with the acid control solution.

4. CONCLUSIONS

In summary, the sensing performance of our spirooxazine derivative, PheSPO, was successfully demonstrated through its applications in drinking water and rice. Among various metal ions, PheSPO showed high selectivity for the detection toward Cu^{2+} and Fe^{3+} with distinct color and spectral changes in acetonitrile. The binding mechanism of **PheSPO** with the targeted metal ions was proposed to be 1:1 stoichiometric complexation and evaluated by means of spectroscopic experiments and DFT calculations. The results showed that the detection limits of the **PheSPO** probe were 0.94 μM for Cu^{2+} and 2.01 μM for Fe^{3+}. Moreover, **PheSPO** was evaluated for its applicability for the analysis of Cu^{2+} and Fe^{3+} in spiked drinking water, and its sensing performance was comparable to that of the standard AAS. Additionally, the strip test of **PheSPO** could also provide a unique colorimetric response when the strip was treated with the digested solution of the rice sample containing Fe^{3+}.

■ ASSOCIATED CONTENT

Supporting Information

The Supporting Information is available free of charge at https://pubs.acs.org/doi/10.1021/acsomega.2c01353.

Effects of solvent polarity, pH conditions for the strip test, crystallographic data of **PheSPO** (deposition number CCDC 2154731), MS spectra of metal−**PheSPO** complexes, list of the dual-sensing probes for Cu^{2+} and Fe^{3+} detection, and ^{1}H and ^{13}C NMR spectra of **PheSPO** (PDF)

https://doi.org/10.1021/acsomega.2c01353
ACS Omega 2022, 7, 18671−18680

AUTHOR INFORMATION

Corresponding Authors

Khomson Suttisintong − *National Nanotechnology Center (NANOTEC), National Science and Technology Development Agency (NSTDA), Khlong Nueng, Pathum Thani 12120, Thailand;* orcid.org/0000-0002-8797-6959; Email: khomson@nanotec.or.th

Weekit Sirisaksoontorn − *Department of Chemistry and Center of Excellence for Innovation in Chemistry, Faculty of Science, Kasetsart University, Bangkok 10900, Thailand; Department of Chemistry, Faculty of Science, Kasetsart University, Bangkok 10900, Thailand;* orcid.org/0000-0001-6902-4519; Email: fsciwks@ku.ac.th

Authors

Supak Pattaweepaiboon − *Department of Chemistry and Center of Excellence for Innovation in Chemistry, Faculty of Science, Kasetsart University, Bangkok 10900, Thailand;* orcid.org/0000-0003-0352-3141

Weerapat Foytong − *Department of Chemistry and Center of Excellence for Innovation in Chemistry, Faculty of Science, Kasetsart University, Bangkok 10900, Thailand; Department of Chemistry, Faculty of Science, Kasetsart University, Bangkok 10900, Thailand*

Natchayapak Phiromphu − *Department of Chemistry, Faculty of Science, Kasetsart University, Bangkok 10900, Thailand*

Tanin Nanok − *Department of Chemistry, Faculty of Science, Kasetsart University, Bangkok 10900, Thailand*

Narongpol Kaewchangwat − *National Nanotechnology Center (NANOTEC), National Science and Technology Development Agency (NSTDA), Khlong Nueng, Pathum Thani 12120, Thailand*

Complete contact information is available at: https://pubs.acs.org/10.1021/acsomega.2c01353

Author Contributions

The article was written through contributions of all authors. All authors have given approval to the final version of the article.

Funding

W.S. acknowledges the Kasetsart University Research and Development (KURDI) under grant no. FF(KU)9.65. K.S. would like to thank the Cluster and Program Management Office (CPMO), the NSTDA-EGAT joint funding scheme under grant no. P1450309.

Notes

The authors declare no competing financial interest.

ACKNOWLEDGMENTS

W.S. would like to thank the Kasetsart University Research and Development Institute (KURDI) and the Centre of Excellence for Innovation in Chemistry (PERCH-CIC), Ministry of Higher Education, Science, Research and Innovation. W.F. also thanks the Human Resource Development in Science Project (Science Achievement Scholarship of Thailand, SAST) for the support.

REFERENCES

(1) Zhu, H.; Fan, J.; Wang, B.; Peng, X. Fluorescent, MRI, and colorimetric chemical sensors for the first-row d-block metal ions. *Chem. Soc. Rev.* **2015**, *44*, 4337−4366.

(2) Zheng, X.; Cheng, W.; Ji, C.; Zhang, J.; Yin, M. Detection of metal ions in biological systems: A review. *Rev. Anal. Chem.* **2020**, *39*, 231−246.

(3) Carter, K. P.; Young, A. M.; Palmer, A. E. Fluorescent sensors for measuring metal ions in living systems. *Chem. Rev.* **2014**, *114*, 4564−4601.

(4) Jaishankar, M.; Tseten, T.; Anbalagan, N.; Mathew, B. B.; Beeregowda, K. N. Toxicity, mechanism and health effects of some heavy metals. *Interdiscip. Toxicol.* **2014**, *7*, 60−72.

(5) Thompson, K. H.; Orvig, C. Boon and bane of metal ions in medicine. *Science* **2003**, *300*, 936−939.

(6) Ali, H.; Khan, E.; Ilahi, I. Environmental chemistry and ecotoxicology of hazardous heavy metals: Environmental persistence, toxicity, and bioaccumulation. *J. Chem.* **2019**, *2019*, 6730305.

(7) Verwilst, P.; Sunwoo, K.; Kim, J. S. The role of copper ions in pathophysiology and fluorescent sensors for the detection thereof. *Chem. Commun.* **2015**, *51*, 5556−5571.

(8) Sharifi-Rad, M.; Anil Kumar, N. V.; Zucca, P.; Varoni, E. M.; Dini, L.; Panzarini, E.; Rajkovic, J.; Tsouh Fokou, P. V.; Azzini, E.; Peluso, I.; Prakash Mishra, A.; Nigam, M.; El Rayess, Y.; Beyrouthy, M. E.; Polito, L.; Iriti, M.; Martins, N.; Martorell, M.; Docea, A. O.; Setzer, W. N.; Calina, D.; Cho, W. C.; Sharifi-Rad, J. Lifestyle, oxidative stress, and antioxidants: back and forth in the pathophysiology of chronic diseases. *Front. Physiol.* **2020**, *11*, 694.

(9) Medeiros, D. M.; Jennings, D. Role of copper in mitochondrial biogenesis via interaction with ATP synthase and cytochrome c oxidase. *J. Bioenerg. Biomembr.* **2002**, *34*, 389−395.

(10) Harris, E. D. Copper transport: An overview. *Exp. Biol. Med.* **1991**, *196*, 130−140.

(11) Vulpe, C.; Levinson, B.; Whitney, S.; Packman, S.; Gitschier, J. Isolation of a candidate gene for Menkes disease and evidence that it encodes a copper transporting ATPase. *Nat. Genet.* **1993**, *3*, 7−13.

(12) Bull, P. C.; Thomas, G. R.; Rommens, J. M.; Forbes, J. R.; Cox, D. W. The Wilson disease gene is a putative copper transporting P-type ATPase similar to the Menkes gene. *Nat. Genet.* **1993**, *5*, 327−337.

(13) Hung, Y. H.; Bush, A. I.; Cherny, R. A. Copper in the brain and Alzheimer's disease. *J. Biol. Inorg Chem.* **2010**, *15*, 61−76.

(14) Bisaglia, M.; Bubacco, L. Copper ions and Parkinson's disease: Why is homeostasis so relevant? *Biomolecules* **2020**, *10*, 195.

(15) Bellion, E. The biological chemistry of the elements: The inorganic chemistry of life. *J. Chem. Educ.* **1992**, *69*, A326.

(16) Tabner, B. J.; Turnbull, S.; El-Agnaf, O. M. A.; Allsop, D. Formation of hydrogen peroxide and hydroxyl radicals from A(beta) and alpha-synuclein as a possible mechanism of cell death in Alzheimer's disease and Parkinson's disease. *Free Radic. Biol. Med.* **2002**, *32*, 1076−1083.

(17) United States Environmental Protection Agency (US EPA). *National Primary Drinking Water Regulations*; Wiley-VCH: Washington, DC, 2009.

(18) United States Environmental Protection Agency (US EPA). *Aquatic Life Ambient Freshwater Quality Criteria-Copper*; Wiley-VCH: Washington, DC, 2007.

(19) Mejía-Rodríguez, F.; Shamah-Levy, T.; Villalpando, S.; García-Guerra, A.; Méndez-Gómez Humarán, I. Iron, zinc, copper and magnesium deficiencies in Mexican adults from the National Health and Nutrition Survey 2006. *Salud Publica Mex.* **2013**, *55*, 275−284.

(20) Şahan, S.; Şahin, U. Determination of copper(II) using atomic absorption spectrometry and Eriochrome blue black R loaded Amberlite XAD-1180 resin. *Clean: Soil, Air, Water* **2010**, *38*, 485−491.

(21) Tautkus, S.; Steponeniene, L.; Kazlauskas, R. Determination of iron in natural and mineral waters by flame atomic absorption spectrometry. *J. Serb. Chem. Soc.* **2004**, *69*, 393−402.

(22) Wainwright, P.; Wadey, D.; Cook, P. An inductively coupled plasma mass spectrometry method for relative free copper determination and generation of a paediatric reference interval. *Ann. Clin. Biochem.* **2018**, *55*, 485−490.

(23) Date, A. R.; Cheung, Y. Y.; Stuart, M. E.; Xiu-Hua, J. Application of inductively coupled plasma mass spectrometry to the analysis of iron ores. *J. Anal. At. Spectrom.* **1988**, *3*, 653−658.
(24) Yan, B.; Worsfold, P. J. Determination of cobalt(II), copper(II) and iron(II) by ion chromatography with chemiluminescence detection. *Anal. Chim. Acta* **1990**, *236*, 287−292.
(25) Kawasaki, N.; Ishigami, A.; Tanimoto, T.; Tanaka, A. Determination of iron(III) ion using ion chromatography with electrochemical detection and its application to the assay of the ferroxidase activity of cerulplasmin. *J. Chromatogr.* **1990**, *503*, 237−243.
(26) Gao, Y.; Wang, L.; Zhuo, J.; Xu, B.; Li, X.; Zhang, J.; Zhang, Z.; Chi, H.; Dong, Y.; Lu, G. A pyrene-based dual chemosensor for colorimetric detection of Cu^{2+} and fluorescent detection of Fe^{3+}. *Tetrahedron Lett.* **2017**, *58*, 3951−3956.
(27) Wang, J.; Wei, T.; Ma, F.; Li, T.; Niu, Q. A novel fluorescent and colorimetric dual-channel sensor for the fast, reversible and simultaneous detection of Fe^{3+} and Cu^{2+} based on terthiophene derivative with high sensitivity and selectivity. *J. Photochem. Photobiol., A* **2019**, *383*, 111982.
(28) Gahlyan, P.; Bawa, R.; Jain, H.; Dalela, M.; Joshi, A.; Ramachandran, C. N.; Prasad, A. K.; Kaur, A.; Kumar, R. Isatin-triazole-functionalized rhodamine: A dual sensor for Cu^{2+} and Fe^{3+} ions and its application to cell imaging. *ChemistrySelect* **2019**, *4*, 7532−7540.
(29) Qian, R.-C.; Long, Y.-T. Wearable chemosensors: A review of recent progress. *ChemistryOpen* **2018**, *7*, 118−130.
(30) Sasaki, Y.; Kubota, R.; Minami, T. Molecular self-assembled chemosensors and their arrays. *Coord. Chem. Rev.* **2021**, *429*, 213607.
(31) Wu, D.; Sedgwick, A. C.; Gunnlaugsson, T.; Akkaya, E. U.; Yoon, J.; James, T. D. Fluorescent chemosensors: the past, present and future. *Chem. Soc. Rev.* **2017**, *46*, 7105−7123.
(32) Soares-Paulino, A. A.; Giroldo, L.; Celante, G.; Lodeiro, C.; Dos Santos, A. A. Formation of an emissive telluroxide promoted by Hg^{2+} in aqueous environment: A new naked-eye and ratiometric rhodamine dimer fluorescent mercury(II) probe. *Dyes Pigm.* **2018**, *159*, 121−127.
(33) Attia, G.; Rahali, S.; Teka, S.; Fourati, N.; Zerrouki, C.; Seydou, M.; Chehimi, S.; Hayouni, S.; Mbakidi, J.-P.; Bouquillon, S.; Majdoub, M.; Chaabane, R. B. Anthracene based surface acoustic wave sensors for picomolar detection of lead ions. Correlation between experimental results and DFT calculations. *Sens. Actuators, B* **2018**, *276*, 349−355.
(34) He, H.; Meng, X.; Deng, L.; Sun, Q.; Huang, X.; Lan, N.; Zhao, F. A novel benzothiadiazole-based and NIR-emissive fluorescent sensor for detection of Hg^{2+} and its application in living cells and zebrafish imaging. *Org. Biomol. Chem.* **2020**, *18*, 6357−6363.
(35) Wang, G.; Xu, W.; Yang, H.; Fu, N. Highly sensitive and selective strategy for imaging Hg^{2+} using near-infrared squaraine dye in live cells and zebrafish. *Dyes Pigm.* **2018**, *157*, 369−376.
(36) Kaur, M.; Choi, D. H.; Cho, M. J. A phenothiazine-based "naked-eye" fluorescent probe for the dual detection of Hg^{2+} and Cu^{2+}: Application as a solid state sensor. *Dyes Pigm.* **2016**, *125*, 1−7.
(37) Vaddypally, S.; Kiselev, V. G.; Byrne, A. N.; Goldsmith, C. F.; Zdilla, M. J. Transition-metal-mediated reduction and reversible double-cyclization of cyanuric triazide to an asymmetric bitetrazolate involving cleavage of the six-membered aromatic ring. *Chem. Sci.* **2021**, *12*, 2268.
(38) Upadhyay, S.; Singh, A.; Sinha, R.; Omer, S.; Negi, K. Colorimetric chemosensors for d-metal ions: A review in the past, present and future prospect. *J. Mol. Struct.* **2019**, *1193*, 89−102.
(39) Kaur, B.; Kaur, N.; Kumar, S. Colorimetric metal ion sensors − A comprehensive review of the years 2011−2016. *Coord. Chem. Rev.* **2018**, *358*, 13−69.
(40) Liuye, S.; Pu, S.; Lu, M.; Cui, S.; Qiu, S. A multi-functional chemosensor for dual channel detection of Arg and colorimetric recognition of Cu^{2+}. *Dyes Pigm.* **2021**, *195*, 109752.
(41) Aysha, T. S.; Mohamed, M. B. I.; El-Sedik, M. S.; Youssef, Y. A. Multi-functional colorimetric chemosensor for naked eye recognition of Cu^{2+}, Zn^{2+} and Co^{2+} using new hybrid azo-pyrazole/pyrrolinone ester hydrazone dye. *Dyes Pigm.* **2021**, *196*, 109795.
(42) Sánchez-Portilloa, P.; Hernández-Sirioa, A.; Godoy-Alcántara, C.; Lacroix, P. G.; Agarwal, V.; Santilláng, R.; Barba, V. Colorimetric metal ion (II) sensors based on imine boronic esters functionalized with pyridine. *Dyes Pigm.* **2021**, *186*, 108991.
(43) Paramonov, S. V.; Lokshin, V.; Fedorova, O. A. Spiropyran, chromene or spirooxazine ligands: Insights into mutual relations between complexing and photochromic properties. *J. Photochem. Photobiol., C* **2011**, *12*, 209−236.
(44) Natali, M.; Aakeröy, C.; Desper, J.; Giordani, S. The role of metal ions and counterions in the switching behavior of a carboxylic acid functionalized spiropyran. *Dalton Trans.* **2010**, *39*, 8269−8277.
(45) Pozzo, J.-L.; Samat, A.; Guglielmetti, R.; Keukeleire, D. D. Solvatochromic and photochromic characteristics of new 1,3-dihydrospiro[2*H*-indole-2, 2'-[2*H*]-bipyrido[3, 2-*f*][2, 3-*h*][1, 4] benzoxazines]. *J. Chem. Soc., Perkin Trans.* **1993**, *2*, 1327−1332.
(46) Pattaweepaiboon, S.; Phiromphu, N.; Kaewchangwat, N.; Suttisintong, K.; Sirisaksoontorn, W. An indolino-spironaphthooxazine probe forcolorimetric detection of ferric ions in drinking water. *New J. Chem.* **2021**, *45*, 11284−11291.
(47) Strokach, Y. P.; Valova, T. M.; Barachevskii, V. A.; Shienok, A. I.; Marevtsev, V. S. Photochromic properties of the bichromophore spirooxazine and its complexes with metal cations. *Russ. Chem. Bull.* **2005**, *54*, 1477−1480.
(48) Huang, Y.; Li, F.; Ye, C.; Qin, M.; Ran, W.; Song, Y. A photochromic sensor microchip for high-performance multiplex metal ions detection. *Sci. Rep.* **2015**, *5*, 9724.
(49) Sahoo, P. R.; Kumar, S. Photochromic spirooxazine as highly sensitive and selective probe for optical detection of Fe^{3+} in aqueous solution. *Sens. Actuators, B* **2016**, *226*, 548−552.
(50) Kopelman, R. A.; Snyder, S. M.; Frank, N. L. Tunable photochromism of spirooxazines via metal coordination. *J. Am. Chem. Soc.* **2003**, *125*, 13684−13685.
(51) Tian, Z.; Stairs, R. A.; Wyer, M.; Mosey, N.; Dust, J. M.; Kraft, T. M.; Buncel, E. Spirooxazine to merooxazine interconversion in the presence and absence of zinc: Approach to a bistable photochemical switch. *J. Phys. Chem. A* **2010**, *114*, 11900−11909.
(52) Ji, J.; Song, G.; Cai, X.; Hu, J.; Feng, L.; Zhu, H. Promoted colorimetric response of spirooxazine derivative: A simple assay for sensitive mercury(II) detection. *Res. Chem. Intermed.* **2016**, *42*, 5597−5605.
(53) Pattaweepaiboon, S.; Nanok, T.; Kaewchangwat, N.; Suttisintong, K.; Sirisaksoontorn, W. Colorimetric detection of Hg^{2+} and CH_3Hg^+ by a novel spirooxazine derivative as a highly sensitive and selective probe. *Dyes Pigm.* **2021**, *186*, 108996.
(54) Becke, A.D., III Density-functional thermochemistry. III. The role of exact exchange. *J. Chem. Phys.* **1993**, *98*, 5648.
(55) Stephens, P. J.; Devlin, F. J.; Chabalowski, C. F.; Frisch, M. J. Ab initio calculation of vibrational absorption and circular dichroism spectra using density functional force fields. *J. Phys. Chem.* **1994**, *98*, 11623−11627.
(56) Grimme, S.; Antony, J.; Ehrlich, S.; Krieg, H. A consistent and accurate ab initio parametrization of density functional dispersion correction (DFT-D) for the 94 elements H-Pu. *J. Chem. Phys.* **2010**, *132*, 154104.
(57) Grimme, S.; Hansen, A.; Brandenburg, J. G.; Bannwarth, C. Dispersion-corrected mean-field electronic structure methods. *Chem. Rev.* **2016**, *116*, 5105−5154.
(58) Barone, V.; Cossi, M. Quantum calculation of molecular energies and energy gradients in solution by a conductor solvent model. *J. Phys. Chem. A* **1998**, *102*, 1995−2001.
(59) Cossi, M.; Rega, N.; Scalmani, G.; Barone, V. Polarizable dielectric model of solvation with inclusion of charge penetration effects. *J. Chem. Phys.* **2001**, *114*, 5691.
(60) Zhurko, G. A. ChemCraft, http://www.chemcraftprog.com (accessed November 25, 2021).
(61) Frisch, M. J.; Trucks, G. W.; Schlegel, H. B.; Scuseria, G. E.; Robb, M. A.; Cheeseman, J. R.; Scalmani, G.; Barone, V.; Mennucci,

https://doi.org/10.1021/acsomega.2c01353
ACS Omega 2022, 7, 18671−18680

B.; Petersson, G. A.; Nakatsuji, H.; Caricato, M.; Li, X.; Hratchian, H. P.; Izmaylov, A. F.; Bloino, J.; Zheng, G.; Sonnenberg, J. L.; Hada, M.; Ehara, M.; Toyota, K.; Fukuda, R.; Hasegawa, J.; Ishida, M.; Nakajima, T.; Honda, Y.; Kitao, O.; Nakai, H.; Vreven, T.; Montgomery, J. A.; Peralta, J. E.; Ogliaro, F.; Bearpark, M.; Heyd, J. J.; Brothers, E.; Kudin, K. N.; Staroverov, V. N.; Keith, T.; Kobayashi, R.; Normand, J.; Raghavachari, K.; Rendell, A.; Burant, J. C.; Iyengar, S. S.; Tomasi, J.; Cossi, M.; Rega, N.; Millam, J. M.; Klene, M.; Knox, J. E.; Cross, J. B.; Bakken, V.; Adamo, C.; Jaramillo, J.; Gomperts, R.; Stratmann, R. E.; Yazyev, O.; Austin, A. J.; Cammi, R.; Pomelli, C.; Ochterski, J. W.; Martin, R. L.; Morokuma, K.; Zakrzewski, V. G.; Voth, G. A.; Salvador, P.; Dannenberg, J. J.; Dapprich, S.; Daniels, A. D.; Farkas, O.; Foresman, J. B.; Ortiz, J. V.; Cioslowski, J.; Fox, D. J. *Gaussian 09*, Revision D.01; Gaussian, Inc.: Wallingford CT, 2013.

(62) di Nunzio, M. R.; Danilov, E. O.; Rodgers, M. A. J.; Favaro, G. Ultrafast excited-state dynamics in some spirooxazines and chromenes. Evidence for a dual relaxation pathway. *Photochem. Photobiol. Sci.* **2010**, *9*, 1391−1399.

https://doi.org/10.1021/acsomega.2c01353
ACS Omega 2022, 7, 18671−18680